
Parallel Spiking Neurons with High Efficiency and Ability to Learn Long-term Dependencies

Wei Fang^{1,2}, Zhaofei Yu³, Zhaokun Zhou^{1,2}, Ding Chen^{4,2}, Yanqi Chen^{1,2},
 Zhengyu Ma², Timothée Masquelier⁵, Yonghong Tian^{1,2}

¹School of Computer Science, Peking University

²Peng Cheng Laboratory

³School of Artificial Intelligence, Peking University

⁴Department of Computer Science and Engineering, Shanghai Jiao Tong University

⁵Centre de Recherche Cerveau et Cognition (CERCO), UMR5549 CNRS - Univ. Toulouse 3

Abstract

Vanilla spiking neurons in Spiking Neural Networks (SNNs) use charge-fire-reset neuronal dynamics, which can only be simulated serially and can hardly learn long-time dependencies. We find that when removing reset, the neuronal dynamics can be reformulated in a non-iterative form and parallelized. By rewriting neuronal dynamics without reset to a general formulation, we propose the Parallel Spiking Neuron (PSN), which generates hidden states that are independent of their predecessors, resulting in parallelizable neuronal dynamics and extremely high simulation speed. The weights of inputs in the PSN are fully connected, which maximizes the utilization of temporal information. To avoid the use of future inputs for step-by-step inference, the weights of the PSN can be masked, resulting in the masked PSN. By sharing weights across time-steps based on the masked PSN, the sliding PSN is proposed to handle sequences of varying lengths. We evaluate the PSN family on simulation speed and temporal/static data classification, and the results show the overwhelming advantage of the PSN family in efficiency and accuracy. To the best of our knowledge, this is the first study about parallelizing spiking neurons and can be a cornerstone for the spiking deep learning research. Our codes are available at <https://github.com/fangwei123456/Parallel-Spiking-Neuron>.

1 Introduction

Spiking Neural Networks (SNNs) are the next generation [1] of Artificial Neural Networks (ANNs) using a lower abstraction of the biological neural system. The spiking neurons are the key components of SNNs, which process input currents with complex neuronal dynamics and fire spikes as outputs when their membrane potential reaches the threshold. The SNNs use discrete spikes to communicate between layers, which enable the event-driven computational paradigm and have extremely high power efficiency in neuromorphic chips such as True North[2], Loihi [3] and Tianjic [4]. Due to their high biological plausibility, SNNs have been regarded by neuroscientists as useful tools for analyzing, simulating, and learning the biological system [5, 6]. With the introduction of deep learning methods [7, 8, 9, 10], the performance of SNNs on real-world tasks has been greatly improved and the applications of SNNs are expanded [11, 12]. As the bridge between neuroscience and computational science, SNNs have attracted more and more research interest in recent years.

The binary characteristic of spikes causes a lot of information losses, which is the main factor leading to the lower accuracy of SNNs than ANNs. Among efforts to bridge the performance gap, the improvement of spiking neurons is a universal approach and has been widely explored [13, 14, 15, 16, 17, 18]. However, previous works are limited to the existing serial charge-fire-reset computing paradigm shown in Fig.1(a), which suffers from slow simulation speed and can hardly learn long-term dependencies.

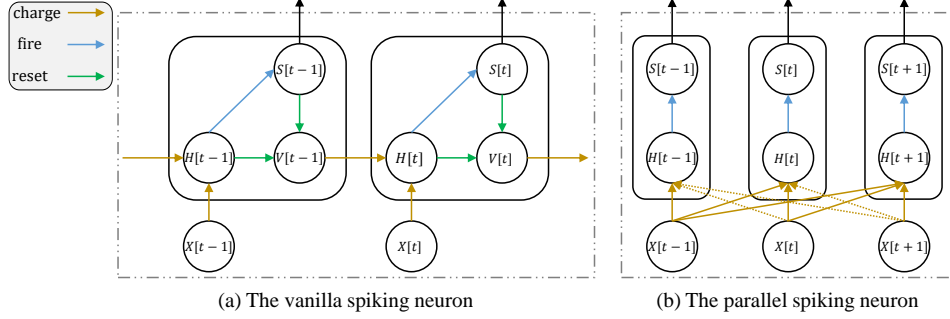


Figure 1: The computational graphs of the vanilla spiking neurons and the parallel spiking neuron. Figure (a) is cited from [13]. The dotted lines in Figure (b) are weights that can be masked for step-by-step computation. $X[t]$, $S[t]$ are the input current and the output spike, and $H[t]$, $V[t]$ are hidden states at time-step t .

In this paper, we propose the Parallel Spiking Neuron (PSN), and its variants the masked PSN as well as the sliding PSN (SPSN). Fig.1(b) shows the computational graph of the PSN, which uses a non-predecessor dependency method to generate hidden states, leading to parallelizable neuronal dynamics and extremely high simulation speed. Since the connections from inputs to $H[t]$ are direct, the PSN has a better learning ability for long-term dependencies than other vanilla spiking neurons. To generate $H[t]$ immediately when $X[t]$ arrives, connections from $X[i]$, $i \geq t+1$ can be masked, as the dotted line shown in Fig.1(b), and then the neuron becomes the masked PSN. The parameters of the masked PSN can also be set as time-invariant, which derives the sliding PSN and is more flexible for input sequences with variable lengths. The main contributions of this paper are as follows:

- 1) We analyze the influence of removing reset from the widely used charge-fire-reset neuronal dynamics, showing that the spiking neuron can be parallelized without reset.
- 2) By rewriting the neuronal dynamics without reset to a general formula, we obtain the PSN with fully parallelizable neuronal dynamics. For step-by-step serial forward and variable length sequences processing, the masked PSN and the sliding PSN are also derived.
- 3) We compare the simulation speed of the PSN family and vanilla spiking neurons, showing an overwhelming performance advantage of the parallel neuronal dynamics. We evaluate the PSN family on sequential, static, and neuromorphic data classification tasks and achieve higher accuracy than previous spiking neurons.

2 Related Work

2.1 Deep Learning for Spiking Neural Networks

The ANN-to-SNN conversion (ANN2SNN) [19, 20, 21] and the surrogate training [22, 23] are the two main deep learning methods for SNNs. The ANN2SNN method uses firing rates in SNNs to approximate the activations in ANNs by converting weights from ANNs to SNNs with extra normalizations to reduce errors. It achieves close performance to that of ANNs in the ImageNet dataset [24], but requires many time-steps to estimate accurate firing rates. The surrogate training method re-defines the gradient of the Heaviside function used in the spike generating process by a smooth and differentiable surrogate function. With the surrogate gradients, the SNNs can be trained by backpropagation through time (BPTT) and gradient descent. The surrogate training method is not based on rate coding as ANN2SNN, resulting in fewer time-steps. However, the use of BPTT during training requires more training time and memory usage than ANN2SNN.

2.2 Improvement of Spiking Neurons

Improving the spiking neurons inspired by biological mechanisms or techniques from ANNs is a practical method. The Parametric Leaky Integrated-and-Fire (PLIF) spiking neuron [13] incorporates learnable membrane time constants and is able to combine the learning of both synapse weights and neuronal dynamics. The gated LIF (GLIF) spiking neuron [14] adds learnable gates to fuse different integration, decay, and reset methods, which enlarges the representation space and increases

the heterogeneity and adaptivity of spiking neurons. The k -based Leaky Integrate-and-Fire (KLIF) neuron [16] adds a learnable scaling factor to adjust the surrogate gradient and applies a ReLU activation to avoid the negative membrane potential. The Multi-Level Firing (MLF) unit [17] contains LIF neurons with thresholds in different levels, which relieves the gradient vanishing problem and improves expression ability. Ponghiran et al. [18] improve the spiking neurons by adding input gates, forget gates, recurrent connections, and multi-bit outputs, which reduce the mismatch between actual and surrogate gradients.

2.3 Improvement of Training Methods and Network Structure

Beyond the spiking neurons, modifying training techniques and network structure are also effective methods to promote the performance of SNNs.

Normalization The threshold-dependent batch normalization (TDBN) [25] normalizes features in both temporal and spatial dimensions and eliminates the variance introduced by thresholds, which is a more suitable normalization method than the batch normalization [26] for SNNs. Batch Normalization Through Time (BNTT) [27] decouples BN along time-steps and uses time-wise parameters, which estimates the distribution of temporal-variant inputs more precisely. Temporal Effective Batch Normalization (TEBN) [28] adds learnable affine transformation on each time-step and has a better ability to capture temporal distributions.

Training Techniques Deep Continuous Local Learning (DECOLLE) [29] uses local losses to avoid BPTT and implements online learning for SNNs. Online training through time (OTTT) [30] approximates iterative gradients with temporal dependencies by eligibility traces updating with time-steps, which also achieves online training and only requires constant training memory agnostic to time-steps. Sparse spiking gradient descent [31] only uses neurons whose membrane potentials are inside a given range for backpropagation, which achieves a speedup and memory reduction in the backward. The attention mechanism on membrane potentials [32] eliminates redundant information, decreases firing rates, and reduces overfitting. Dspike [33] uses the finite difference to estimate gradients and achieves higher accuracy than plain surrogate gradient methods. The temporal efficient training (TET) [34] calculates loss at each time-step and averages them rather than using averaged outputs to calculate loss, which improves the temporal scalability of SNNs.

Network Structure Spike-Element-Wise ResNet [35] solves the gradient vanishing/exploding problems of the plain Spiking ResNet caused by sigmoid-like surrogate functions, which successfully trained the first deep SNN with more than 150 layers. Spikformer [36] modifies the softmax-based self-attention in Transformer [37] to the spike-based formulation, which is appropriate for SNNs and achieves state-of-the-art accuracy on the ImageNet dataset.

2.4 Acceleration for Sequence Processing

Massively parallel computing with graphics processing units (GPUs) [38] is one of the key factors that drives deep learning research. However, the serial computing characteristic of the recurrent structure such as SNNs and Recurrent Neural Networks (RNNs) can not fully exploit the parallel computing power of GPUs. To accelerate the sequence processing, convolution-based methods [39, 40] discard the recurrent structure and employ the convolutional layers, which are fully parallelized during training on GPUs. The gated impulse linear recurrent network [41] is another solution that uses the Parallel Prefix Sum (Scan) algorithm [42] to parallelize linear recurrences. The transformer [37] replaces recurrences with self-attention and positional encoding, which achieves faster training speed than recurrent and convolutional encoder-decoder structures.

3 Methods

In this section, we introduce the motivation of removing neuronal reset, the idea of generalizing spiking neurons without reset as the PSN, and the derivation of the masked PSN and the sliding PSN. Note that we use regular letters such as X to represent scalars, and bold letters such as \mathbf{X} to represent tensors.

3.1 Vanilla Spiking Neurons W/WO Reset

Spiking neurons in SNNs have rich neuronal dynamics, which endow SNNs with temporal information processing ability. In most cases, the behaviors of spiking neurons can be described by three discrete-time equations [13]:

$$H[t] = f(V[t-1], X[t]), \quad (1)$$

$$S[t] = \Theta(H[t] - V_{th}), \quad (2)$$

$$V[t] = \begin{cases} H[t] \cdot (1 - S[t]) + V_{reset} \cdot S[t], & \text{hard reset} \\ H[t] - V_{th} \cdot S[t], & \text{soft reset} \end{cases}, \quad (3)$$

where $X[t]$ is the input current, $H[t]$ is the membrane potential after charging but before firing, $V[t]$ is the membrane potential after firing, and $S[t]$ is the output spike at time-step t . V_{th} in Eq.(2) is the threshold potential, and V_{reset} in Eq.(3) is the reset potential. $\Theta(x)$ is the Heaviside step function and $\Theta(x) = 1$ for all $x \geq 0$, otherwise $\Theta(x) = 0$. Eq.(1) is the neuronal charging equation, and f is specific to different spiking neurons. After charging, $H[t]$ will be compared to V_{th} and determine whether to fire spikes, which is described by Eq.(2). After firing, the membrane potential will be reset, as Eq.(3) shows. Note that there are two kinds of resets, which are the hard reset and the soft reset. If the neuron fires, the hard reset will set $V[t]$ to V_{reset} , while the soft reset will decrease $V[t]$ by V_{th} . The hard reset is widely used in surrogate training for better performance observed in experiments [43], while the soft reset is preferred in ANN2SNN for lower conversion errors. When simulating SNNs, the iterative process following Eqs.(1)-(3) over time-steps is employed, which has a time complexity of $\mathcal{O}(T)$, where T is the number of time-steps.

For frequently-used spiking neurons, Eq.(1) is linear and can be reformulated to a non-iterative equation if we can ignore Eq.(3) in some cases, e.g., in the subthreshold regime $H[t] < V_{th}$ for all t . Then $V[t] = H[t]$ at all t and we will only use $H[t]$ in this case. More specifically, we take the Integrate-and-Fire (IF) neuron and the Leaky Integrate-and-Fire (LIF) neuron as examples. For simplicity, suppose $H[-1] = 0$ for both types of neurons, and the resting potential for the LIF neuron is 0. The neuronal charge equation, or Eq.(1), for the IF neuron is

$$H[t] = H[t-1] + X[t]. \quad (4)$$

And Eq.(4) can be easily reformulated as

$$H[t] = \sum_{i=0}^t X[i]. \quad (5)$$

The neuronal charge equation for the LIF neuron is

$$H[t] = (1 - \frac{1}{\tau_m}) \cdot V[t-1] + \frac{1}{\tau_m} \cdot X[t], \quad (6)$$

where τ_m is the membrane time constant. Eq.(6) can also be reformulated as

$$H[t] = \frac{1}{\tau_m} \cdot \sum_{i=0}^t (1 - \frac{1}{\tau_m})^{t-i} \cdot X[i]. \quad (7)$$

With the non-iterative equations, $H[t]$ at all time-steps, or $\mathbf{H} = \{H[0], H[1], \dots, H[T-1]\}$, can be calculated in parallel. For each $H[t]$ obtained by the cumulative sum operation, the time complexity can be as low as $\mathcal{O}(\log(t)) \leq \mathcal{O}(\log(T))$ when using the Parallel Prefix Sum (Scan) algorithm. When \mathbf{H} is given, the element-wise operation Eq.(2) can also be applied on the whole \mathbf{H} and the time complexity is $\mathcal{O}(1)$ in devices that support parallel computing such as the CUDA devices. Thus, the whole time complexity for the neuronal charging and firing reduces to $\mathcal{O}(\log(T))$ when we can ignore the neuronal resetting.

So, how can we ignore neuronal resetting? A possible method is setting $V_{th} = +\infty$ to make Eq.(3) become an identity function. However, the neuron can only output 0 in this case, which is meaningless. Another method is to remove the neuronal resetting directly from the neuronal dynamics, which means only using Eq.(1) and Eq.2. This crude and simple method may raise further concerns that the absence of neuronal resetting will cause the neuron to fire uninterruptedly. Note that the firing rate is determined by inputs, charging, thresholds, and resetting. Thus, the effect of only removing reset on firing rates is not deterministic. In addition, the experiment results in the next section will show that the uninterrupted firing issue will not occur.

3.2 Parallel Spiking Neuron

After removing neuronal resetting, the charging equation of the spiking neuron can be formulated into a non-iterative equation, and the solution for $H[t]$ becomes a cumulative sum operation. It can be found that Eq.(5) and Eq.(7) are two specific cases of a linear combination of $X[t]$. More specifically, we formulate a general linear combination as

$$H[t] = \sum_{i=0}^{T-1} W_{t,i} \cdot X[i], \quad (8)$$

where $W_{t,i}$ is the weight between $X[i]$ and $H[t]$. Then, $W_{t,i} = \Theta(t - i)$ for the IF neuron without reset, and $W_{t,i} = \frac{1}{\tau_m} (1 - \frac{1}{\tau_m})^{t-i} \cdot \Theta(t - i)$ for the LIF neuron without reset. Based on the above analysis, we propose the Parallel Spiking Neuron (PSN), whose neuronal dynamics are as follows:

$$\mathbf{H} = \mathbf{W} \mathbf{X}, \quad \mathbf{W} \in \mathbb{R}^{T \times T}, \mathbf{X} \in \mathbb{R}^{T \times N} \quad (9)$$

$$\mathbf{S} = \Theta(\mathbf{H} - \mathbf{B}), \quad \mathbf{B} \in \mathbb{R}^T, \mathbf{S} \in \{0, 1\}^{T \times N} \quad (10)$$

where \mathbf{X} is the input sequence, \mathbf{W} is the learnable weight matrix, \mathbf{H} is the hidden state sequence, \mathbf{B} is the learnable threshold, and \mathbf{S} is the binary output spike sequence. N is the number of batch size, and T is the number of time-steps. Note that \mathbf{W} is a $T \times T$ matrix, indicating that $H[t]$ can integrate the information from all time-steps directly, rather than that of the last one or two time-steps. Thus, the PSN is a T -order neuron. No iterative equation is used, and the computation of PSN is fully parallel. The time complexity of the PSN is determined by Eq.(9), which is a matrix-matrix multiplication. The simulation of PSN is much faster than that of vanilla spiking neurons because the matrix-matrix multiplication is highly optimized in linear algebra libraries such as Intel MKL and cuBLAS. BPTT is still used during training, but also in a parallel, rather than a serial formulation.

3.3 Masked k -Order Parallel Spiking Neuron

The high-order characteristic of the PSN is also a double-edged sword. The output sequence \mathbf{S} can only be generated when all $X[t]$ have arrived, indicating that each spiking neuron layer will increase latency T to the whole SNN. Such a latency problem is also reported on the time-to-first-spike SNNs [44, 45, 46, 47]. Note that although the latency is unavoidable, the throughput can still approach the plain SNN with the multi-stage pipeline [44, 45]. To solve the latency problem of the PSN, we add a mask \mathbf{M}_k to multiply \mathbf{W} element-wise before generating \mathbf{H} and propose the k -order masked PSN, whose neuronal charging equation is

$$\mathbf{H} = (\mathbf{W} \cdot \mathbf{M}_k) \mathbf{X}, \quad \mathbf{W} \in \mathbb{R}^{T \times T}, \mathbf{M}_k \in \mathbb{R}^{T \times T}, \mathbf{X} \in \mathbb{R}^{T \times N} \quad (11)$$

where \mathbf{M}_k is defined as

$$\mathbf{M}_k[i][j] = \begin{cases} 1, & j \leq i \leq j + k - 1 \\ 0, & \text{otherwise} \end{cases} \quad (12)$$

With the mask \mathbf{M}_k , $H[t]$ depends only on the latest k inputs $\{X[t - k + 1], \dots, X[t - 1], X[t]\}$ and $S[t]$ can be computed and sent to the next layer once $X[t]$ is received.

When training the k -order masked PSN, the progressive masking method is employed, which uses an all-ones matrix $\mathbf{1}$ as the mask first, and gradually replaces $\mathbf{1}$ with \mathbf{M}_k . More specifically, we use

$$\mathbf{M}_k(\lambda) = \lambda \cdot \mathbf{M}_k + (1 - \lambda) \cdot \mathbf{1} \quad (13)$$

as the mask, and λ increases from 0 to 1 during training. In the early stages of training, $\mathbf{M}_k(\lambda) \approx \mathbf{1}$, indicating that the future information can be exploited to provide appropriate primary parameters and help the network converge.

3.4 k -Order Sliding Parallel Spiking Neuron

The parameters of the PSN and the masked PSN are time-wise, which require extra operations for processing sequences with variable lengths. To solve this issue, we modify the parameters to be

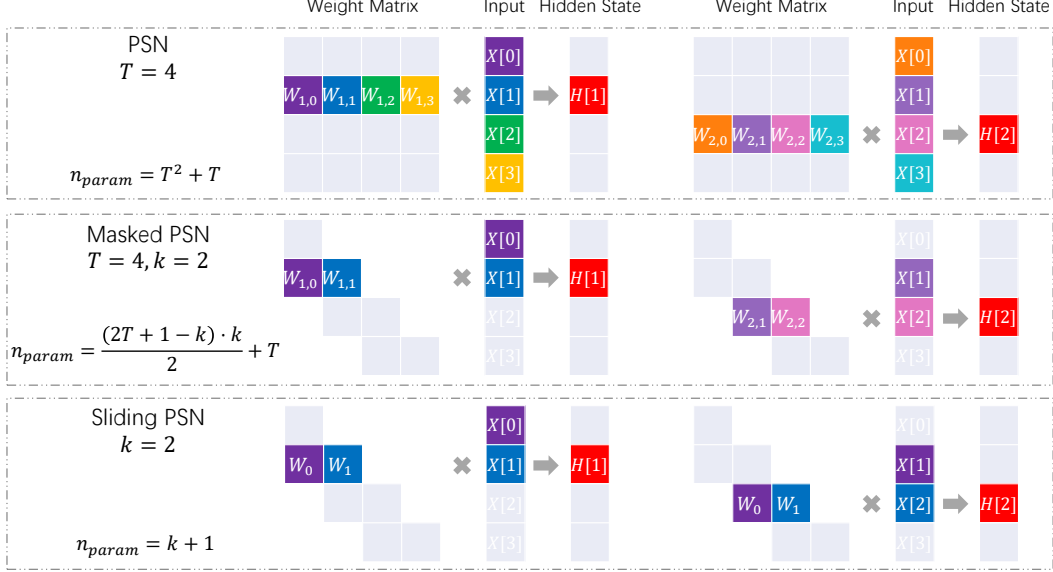


Figure 2: Comparison of the PSN family on the parameter number n_{param} and the generation of hidden states.

shared across time-steps and propose the k -order sliding PSN (SPSN), whose neuronal dynamics are

$$H[t] = \sum_{i=0}^{k-1} W_i \cdot X[t - k + 1 + i], \quad (14)$$

$$S[t] = \Theta(H[t] - V_{th}), \quad (15)$$

where $\mathbf{W} = [W_0, W_1, \dots, W_{k-1}] \in \mathbb{R}^k$ is the learnable weight, $X[j] = 0$ for all $j < 0$, and V_{th} is the learnable threshold. Similar to the masked PSN, $H[t]$ of the SPSN depends only on the latest k inputs as well. More specifically, the weight slides over inputs and generates hidden states, which is a standard 1D convolution operation. Additionally, it can also be implemented by matrix-matrix multiplication. When the input sequence $\mathbf{X} \in \mathbb{R}^{T \times N}$ arrives and its length T is known, the matrix $\mathbf{A} \in \mathbb{R}^{T \times T}$ can be generated as

$$\mathbf{A}[i][j] = \begin{cases} W_{k-1-i+j}, & i + 1 - k \leq j \leq i \\ 0, & \text{otherwise} \end{cases}, \quad (16)$$

then $\mathbf{H} = \mathbf{AX}$. According to the results of our experiments, using matrix-matrix multiplication is faster than using convolution.

3.5 Summary of the PSN Family

As a summary, Fig.2 shows the comparison of the parameter number n_{param} and the generation of hidden states of the PSN family. Remarkably, using the PSN in deep SNNs will add a negligible number of parameters because T is small in directly trained SNNs. For example, using the PSN with $T = 4$ will add 340 and 200 parameters in spiking ResNet-18 and VGG-11, which only increase 0.00291% and 0.00015% parameters of the original SNNs. Additionally, the PSN family has only one hidden state \mathbf{H} , making them consume less memory than the vanilla spiking neurons with at least two hidden states \mathbf{H}, \mathbf{V} during training, which are analyzed and verified by experiments in the supplementary materials.

4 Experiments

In this section, we report the experiment results of evaluating the PSN family in aspects of simulation performance and temporal/static data classifying accuracy. All experiments are based on the SpikingJelly [48] framework. The details of the training are provided in the supplementary materials.

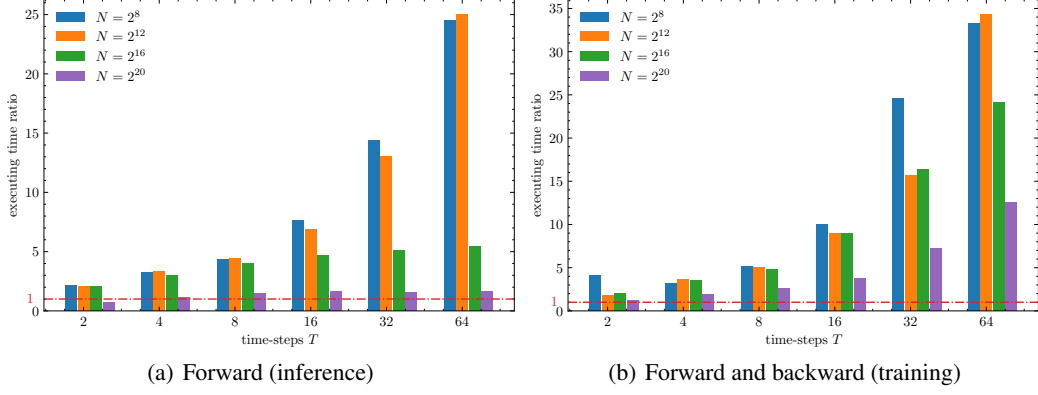


Figure 3: The executing time ratio of the LIF neuron and the PSN for one forward in inference and one forward and backward in training.

Neuron \ Dataset	PSN	masked PSN	SPSN	GLIF[14]	KLIF[16]	PLIF[13]	LIF	LIF wo reset
Sequential CIFAR10	88.45	85.81	86.70	83.66	83.26	83.49	81.50	79.50
Sequential CIFAR100	62.21	60.69	62.11	58.92	57.37	57.55	55.45	53.33

Table 1: The test accuracy (%) of different spiking neurons on sequential CIFAR.

4.1 Simulation Speed Benchmark

We evaluated the simulation speed benchmark of the PSN and the LIF neuron, which is widely used in deep SNNs and acts as the baseline of the vanilla spiking neurons. Note that the implementations and simulation speed of the masked PSN and the SPSN are almost identical to the PSN. Thus, we take the PSN as the benchmark for the PSN family. The benchmark is running in two modes, which are inference and training. In inference, we use the PyTorch just-in-time (JIT) compiling to fuse Eq.(1)-(3) of the LIF neuron across all time-steps into a single function to accelerate by avoiding the calling overhead of too many tiny CUDA kernels. However, PyTorch JIT does not support modifying the backward for a fused forward function, so the surrogate method used in the backward of Eq.(2) breaks the fusion of all three equations in training. Thus, we have to use three smaller JIT functions at each time-step for the LIF neuron in training. For the PSN, there is no difference between the implementations for inference and training, which both involve a matrix-matrix multiplication and an element-wise operation. We tested the neuron numbers $N = 2^8, 2^{12}, 2^{16}, 2^{20}$ and the time-step numbers $T = 2, 4, 8, 16, 32, 64$, which are typical options for deep SNNs. Denote the executing time of two neurons as t_{PSN} and t_{LIF} respectively, then the ratio $\frac{t_{LIF}}{t_{PSN}}$ is shown in Fig.3. It can be found that in most cases, the simulation of the PSN is much faster than that of the LIF neuron.

4.2 Learning Long-term Dependencies

To verify the learning ability for long-term dependencies of different spiking neurons, we evaluated their performance on classifying sequential CIFAR10 and CIFAR100. In these tasks, the image will be sent to the SNN column by column, which is similar to how humans read from left to right. The sequential image classification task is widely used to evaluate the learning ability of a network for long-term dependencies. The network structure is modified from [13] by replacing 2D convolutional/max pooling layers with 1D convolutional and average pooling layers, and removing the voting layers. Due to the column-by-column input, T is 32, which is the width of the image. The compared neurons include the PSN, 32-order masked PSN, 32-order SPSN, GLIF with channel-wise parameters, KLIF, PLIF, and the LIF neuron w/wo reset. We use the optimal reset options determined by ablation experiments for different neurons, which are using soft reset and detach reset [49] for the PLIF and LIF neurons, and using soft reset for the KLIF neuron. The GLIF neuron uses learnable gates to control all options, which do not need to be set manually. For the masked PSN, $\lambda = \min(1, 8 \cdot epoch / (epochs - 1))$, where $epoch$ denotes the current training epoch, and $epochs$ denotes the total number of epochs.

Tab.1 shows the accuracy of all neurons on sequential CIFAR. It can be found that the rank of accuracy is PSN > SPSN > masked PSN > GLIF > PLIF > KLIF > LIF > LIF wo reset, which is as expected. The PSN exploits information from all time-steps and has the highest learning ability, but it may be

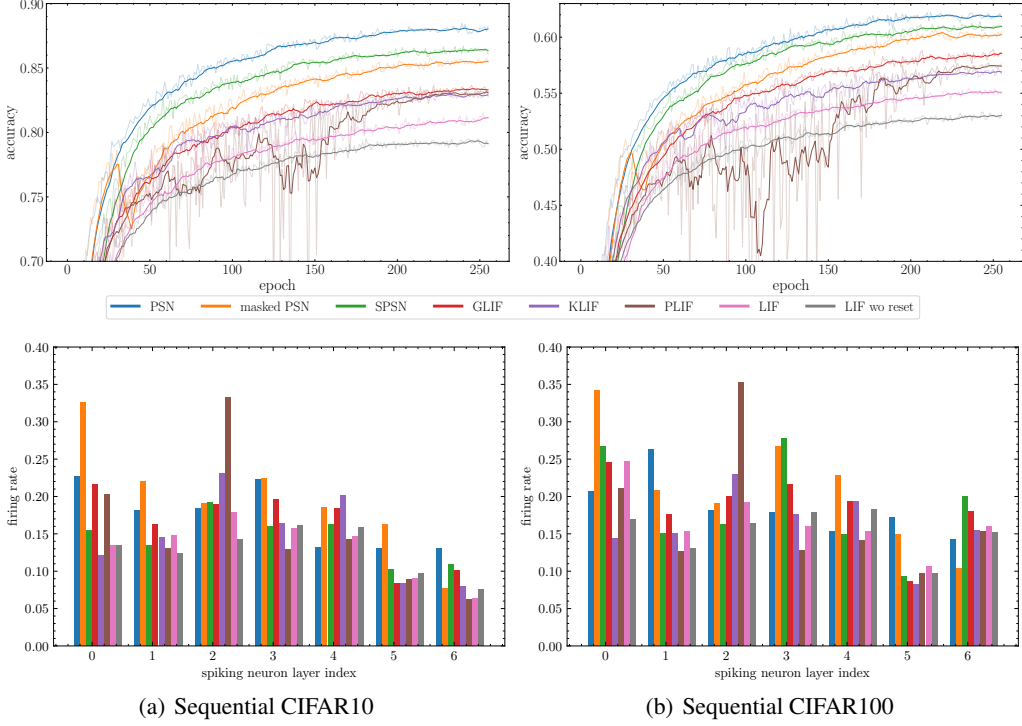


Figure 4: The accuracy curves and firing rates of different neurons for classifying sequential CIFAR.

criticized for unfair comparison because it can read all columns at once. Therefore, the accuracy of the masked PSN and the SPSN is more convincing because they can still run in a step-by-step mode. Due to the introduction of high-order information, they work better than any other traditional spiking neurons. Meanwhile, the GLIF neuron is the best among traditional spiking neurons, indicating that fusing different kinds of charging, decaying, and resetting increases learning ability. The LIF neuron without reset has lower accuracy than the LIF neuron, indicating that the direct removal of reset drops the learning ability of the vanilla spiking neurons. Thus, using high-order information as the PSN family is necessary to fix this decline.

To make clear comparisons, we plotted the accuracy curves during training and firing rates of each spiking neuron layer of trained SNNs with different spiking neurons, as shown in Fig.4. These accuracy curves are the moving averages of 8 epochs, and the light-colored curves show the original accuracy. The curves of the PSN family are almost always above other curves, which clearly show their superior performance on convergence speed and final accuracy. Note that there is a sharp drop in the curves of the masked PSN around epoch 32, which is caused by the mask becoming completely binary. The firing rates indicate that uninterrupted firing does not occur with the removal of neuronal resetting. In general, the PSN and the masked PSN are more easily to be activated and show higher firing rates than others. Meanwhile, the firing rates of the SPSN and the LIF neuron without reset are slightly higher than the vanilla spiking neurons. Thus, we conclude that removal of reset does increase firing rates, but the increment degree depends on the neuron's structure. On the other hand, considering the huge improvement in simulation efficiency and long-term dependencies learning ability, the slightly higher firing rate is acceptable.

Fig.5 shows the accuracy-order curve on the sequential CIFAR100 dataset for the masked PSN and SPSN, with the highest accuracy marked by a red \star . It can be seen that when the order increases from 1 to 4, the accuracy improves quickly. When we continue to increase the order, the improvement is marginal and the accuracy even drops. The highest accuracy is obtained by a large, but not the largest order, which is 20 and 31 for the masked PSN and SPSN, respectively. But in most cases, high accuracy can be guaranteed with $k = T$. Remarkably, the SPSN curve is almost always above the masked PSN curve, and excels the PSN when $k = 21$ and $k = 31$, indicating that the time-invariant parameters have better generalization ability to process temporal information.

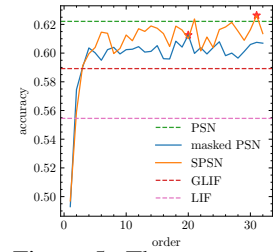


Figure 5: The accuracy-order curve of the sequential CIFAR100.

Dataset	Method	Spiking Network	Time-steps	Accuracy(%)
CIFAR10	Dspike[33]	Modified ResNet-18	6	94.25
	TET[34]	ResNet-19	6	94.50
	TDBN[25]	ResNet-19	6	93.16
	TEBN[28]	ResNet-19	6	94.71
	PLIF[13]	PLIF Net	8	93.50
	KLIF[16]	Modified PLIF Net	10	92.52
	GLIF[14]	ResNet-19	6	95.03
ImageNet	PSN	Modified PLIF Net	4	95.32
	Dspike[33]	ResNet-34	6	68.19
		VGG-16	5	71.24
	TET[34]	SEW ResNet-34	4	68.00
	TDBN[25]	ResNet-34 with double channels	6	67.05
	TEBN[28]	SEW ResNet-34	4	68.28
	GLIF[14]	ResNet-34	4	67.52
	SEW ResNet[35]	SEW ResNet-18	4	63.18
		SEW ResNet-34	4	67.04
	PSN	SEW ResNet-18	4	67.63
		SEW ResNet-34	4	70.54
	Dspike[33]	ResNet-18	10	75.40
	TET[34]	VGG	10	83.17
	TDBN[25]	ResNet-19	10	67.80
	TEBN[28]	VGG	10	84.90
CIFAR10-DVS	PLIF[13]	PLIF Net	20	74.80
	KLIF[16]	Modified PLIF Net	15	70.90
	GLIF[14]	Wide 7B Net	16	78.10
	SEW ResNet[35]	Wide 7B Net	16	74.40
	SPSN ($k = 2$)	VGG	4, 8, 10	82.30, 85.30, 85.90

Table 2: Comparison of the PSN family and other methods.

4.3 Static and Neuromorphic Data Classification

Static and neuromorphic data classification tasks are also common benchmarks for SNNs. We evaluated the PSN family on the static CIFAR10, ImageNet datasets, and the neuromorphic CIFAR10-DVS [50] dataset. The number of time-steps for static datasets is small, and the latency is not the main issue. Thus, we use the PSN in CIFAR10 and ImageNet. According to the results on sequential CIFAR, the SPSN uses fewer parameters but gets higher accuracy, and we will use it for CIFAR10-DVS. The results are listed in Tab.2.

CIFAR10 We modified the network structure of [13], or the PLIF Net, by using average pooling and removing voting layers. Our PSN uses the shortest time-steps $T = 4$ and achieves the highest accuracy of 95.32%.

ImageNet We used the SEW ResNet [35] for classifying the ImageNet dataset. We verified the performance of the SNN on SEW ResNet-18/34 and got a stable 3% accuracy improvement over the original SEW ResNet with the IF neuron. Our method achieves 70.54% accuracy and is only second to the Dspike method using one more time-step and VGG-16, which has a number of parameters 6.3 times as many as ours.

CIFAR10-DVS We used the VGG structure from [34]. Considering the fact that the DVS data contains temporal features and T is larger than the static datasets, we use the 2-order SPSN. We achieve 82.3 % accuracy with $T = 4$, which is the first work to get 80+% accuracy in such few time-steps. When increasing time-steps to $T = 8$, we achieve 85.30% accuracy, which is 2+% higher than that of the previous SOTA method [28] and we use two fewer time-steps. With $T = 10$, the accuracy is further improved to 85.90%.

5 Conclusion

In this paper, we remove reset from neuronal dynamics of vanilla spiking neurons and propose the PSN family, including the PSN, the masked PSN, and sliding PSN. The PSN family can be simulated in parallel, which greatly accelerates the training of deep SNNs. Weights of inputs in the PSN family can be fully connected, or masked/shared with a custom order. Experimental results of simulation speed and temporal/static data classification verify the efficiency and accuracy of the PSN family when compared with previous spiking neurons. Our work may be a milestone as well as a cornerstone for modern spiking neurons.

References

- [1] Wolfgang Maass. Networks of spiking neurons: the third generation of neural network models. *Neural Networks*, 10(9):1659–1671, 1997.
- [2] Paul A Merolla, John V Arthur, Rodrigo Alvarez-Icaza, Andrew S Cassidy, Jun Sawada, Filipp Akopyan, Bryan L Jackson, Nabil Imam, Chen Guo, Yutaka Nakamura, et al. A million spiking-neuron integrated circuit with a scalable communication network and interface. *Science*, 345(6197):668–673, 2014.
- [3] Mike Davies, Narayan Srinivasa, Tsung-Han Lin, Gautham Chinya, Yongqiang Cao, Sri Harsha Choday, Georgios Dimou, Prasad Joshi, Nabil Imam, Shweta Jain, Yuyun Liao, Chit-Kwan Lin, Andrew Lines, Ruokun Liu, Deepak Mathai, Steven McCoy, Arnab Paul, Jonathan Tse, Guruguanthan Venkataraman, Yi-Hsin Weng, Andreas Wild, Yoonseok Yang, and Hong Wang. Loihi: A neuromorphic manycore processor with on-chip learning. *IEEE Micro*, 38(1):82–99, 2018.
- [4] Jing Pei, Lei Deng, Sen Song, Mingguo Zhao, Youhui Zhang, Shuang Wu, Guanrui Wang, Zhe Zou, Zhenzhi Wu, Wei He, et al. Towards artificial general intelligence with hybrid tianjic chip architecture. *Nature*, 572(7767):106–111, 2019.
- [5] Chris Eliasmith, Terrence C. Stewart, Xuan Choo, Trevor Bekolay, Travis DeWolf, Yichuan Tang, and Daniel Rasmussen. A large-scale model of the functioning brain. *Science*, 338(6111):1202–1205, 2012.
- [6] Marcel Stimberg, Romain Brette, and Dan FM Goodman. Brian 2, an intuitive and efficient neural simulator. *eLife*, 8:e47314, 2019.
- [7] Emre O Neftci, Hesham Mostafa, and Friedemann Zenke. Surrogate gradient learning in spiking neural networks: Bringing the power of gradient-based optimization to spiking neural networks. *IEEE Signal Processing Magazine*, 36(6):51–63, 2019.
- [8] Amirhossein Tavanaei, Masoud Ghodrati, Saeed Reza Kheradpisheh, Timothée Masquelier, and Anthony Maida. Deep learning in spiking neural networks. *Neural Networks*, 111:47–63, 2019.
- [9] Yongqiang Cao, Yang Chen, and Deepak Khosla. Spiking deep convolutional neural networks for energy-efficient object recognition. *International Journal of Computer Vision*, 113(1):54–66, 2015.
- [10] Bodo Rueckauer, Iulia-Alexandra Lungu, Yuhuang Hu, Michael Pfeiffer, and Shih-Chii Liu. Conversion of continuous-valued deep networks to efficient event-driven networks for image classification. *Frontiers in Neuroscience*, 11:682, 2017.
- [11] Kaushik Roy, Akhilesh Jaiswal, and Priyadarshini Panda. Towards spike-based machine intelligence with neuromorphic computing. *Nature*, 575(7784):607–617, 2019.
- [12] Rui Yuan, Qingxi Duan, Pek Jun Tiw, Ge Li, Zhuojian Xiao, Zhaokun Jing, Ke Yang, Chang Liu, Chen Ge, Ru Huang, et al. A calibratable sensory neuron based on epitaxial vo2 for spike-based neuromorphic multisensory system. *Nature Communications*, 13(1):1–12, 2022.
- [13] Wei Fang, Zhaofei Yu, Yanqi Chen, Timothée Masquelier, Tiejun Huang, and Yonghong Tian. Incorporating learnable membrane time constant to enhance learning of spiking neural networks. In *Proceedings of the IEEE/CVF International Conference on Computer Vision (ICCV)*, pages 2661–2671, 2021.
- [14] Xingting Yao, Fanrong Li, Zitao Mo, and Jian Cheng. GLIF: A unified gated leaky integrate-and-fire neuron for spiking neural networks. In Alice H. Oh, Alekh Agarwal, Danielle Belgrave, and Kyunghyun Cho, editors, *Advances in Neural Information Processing Systems (NeurIPS)*, 2022.
- [15] Ilyass Hammouamri, Timothée Masquelier, and Dennis George Wilson. Mitigating catastrophic forgetting in spiking neural networks through threshold modulation. *Transactions on Machine Learning Research*, 2022.
- [16] Chunming Jiang and Yilei Zhang. Klif: An optimized spiking neuron unit for tuning surrogate gradient slope and membrane potential, 2023.
- [17] Lang Feng, Qianhui Liu, Huajin Tang, De Ma, and Gang Pan. Multi-level firing with spiking ds-resnet: Enabling better and deeper directly-trained spiking neural networks. In Lud De Raedt, editor, *International Joint Conferences on Artificial Intelligence Organization (IJCAI)*, pages 2471–2477, 7 2022. Main Track.

[18] Wachirawit Ponghiran and Kaushik Roy. Spiking neural networks with improved inherent recurrence dynamics for sequential learning. In *Proceedings of the AAAI Conference on Artificial Intelligence (AAAI)*, volume 36, pages 8001–8008, 2022.

[19] Tong Bu, Wei Fang, Jianhao Ding, PengLin Dai, Zhaofei Yu, and Tiejun Huang. Optimal ann-snn conversion for high-accuracy and ultra-low-latency spiking neural networks. In *International Conference on Learning Representations (ICLR)*, 2021.

[20] Shikuang Deng and Shi Gu. Optimal conversion of conventional artificial neural networks to spiking neural networks. In *International Conference on Learning Representations (ICLR)*, 2021.

[21] Bing Han, Gopalakrishnan Srinivasan, and Kaushik Roy. Rmp-snn: Residual membrane potential neuron for enabling deeper high-accuracy and low-latency spiking neural network. In *Proceedings of the IEEE/CVF Conference on Computer Vision and Pattern Recognition (CVPR)*, pages 13558–13567, 2020.

[22] Yujie Wu, Lei Deng, Guoqi Li, Jun Zhu, and Luting Shi. Spatio-temporal backpropagation for training high-performance spiking neural networks. *Frontiers in Neuroscience*, 12, 2018.

[23] Sumit Bam Shrestha and Garrick Orchard. Slayer: Spike layer error reassignment in time. In *Advances in Neural Information Processing Systems (NeurIPS)*, pages 1419–1428, 2018.

[24] Olga Russakovsky, Jia Deng, Hao Su, Jonathan Krause, Sanjeev Satheesh, Sean Ma, Zhiheng Huang, Andrej Karpathy, Aditya Khosla, Michael Bernstein, et al. Imagenet large scale visual recognition challenge. *International Journal of Computer Vision*, 115(3):211–252, 2015.

[25] Hanle Zheng, Yujie Wu, Lei Deng, Yifan Hu, and Guoqi Li. Going deeper with directly-trained larger spiking neural networks. In *Proceedings of the AAAI Conference on Artificial Intelligence (AAAI)*, volume 35, pages 11062–11070, 2021.

[26] Sergey Ioffe and Christian Szegedy. Batch normalization: Accelerating deep network training by reducing internal covariate shift. In *International Conference on Machine Learning (ICML)*, pages 448–456. PMLR, 2015.

[27] Youngeun Kim and Priyadarshini Panda. Revisiting batch normalization for training low-latency deep spiking neural networks from scratch. *Frontiers in Neuroscience*, 15, 2021.

[28] Chaoteng Duan, Jianhao Ding, Shiyan Chen, Zhaofei Yu, and Tiejun Huang. Temporal effective batch normalization in spiking neural networks. In Alice H. Oh, Alekh Agarwal, Danielle Belgrave, and Kyunghyun Cho, editors, *Advances in Neural Information Processing Systems (NeurIPS)*, 2022.

[29] Jacques Kaiser, Hesham Mostafa, and Emre Neftci. Synaptic plasticity dynamics for deep continuous local learning (decolle). *Frontiers in Neuroscience*, 14, 2020.

[30] Mingqing Xiao, Qingyan Meng, Zongpeng Zhang, Di He, and Zhouchen Lin. Online training through time for spiking neural networks. In Alice H. Oh, Alekh Agarwal, Danielle Belgrave, and Kyunghyun Cho, editors, *Advances in Neural Information Processing Systems (NeurIPS)*, 2022.

[31] Nicolas Perez-Nieves and Dan F. M. Goodman. Sparse spiking gradient descent. In A. Beygelzimer, Y. Dauphin, P. Liang, and J. Wortman Vaughan, editors, *Advances in Neural Information Processing Systems (NeurIPS)*, 2021.

[32] Man Yao, Guanshe Zhao, Hengyu Zhang, Yifan Hu, Lei Deng, Yonghong Tian, Bo Xu, and Guoqi Li. Attention spiking neural networks. *IEEE Transactions on Pattern Analysis and Machine Intelligence*, pages 1–18, 2023.

[33] Yuhang Li, Yufei Guo, Shanghang Zhang, Shikuang Deng, Yongqing Hai, and Shi Gu. Differentiable spike: Rethinking gradient-descent for training spiking neural networks. In A. Beygelzimer, Y. Dauphin, P. Liang, and J. Wortman Vaughan, editors, *Advances in Neural Information Processing Systems (NeurIPS)*, 2021.

[34] Shikuang Deng, Yuhang Li, Shanghang Zhang, and Shi Gu. Temporal efficient training of spiking neural network via gradient re-weighting. In *International Conference on Learning Representations (ICLR)*, 2022.

[35] Wei Fang, Zhaofei Yu, Yanqi Chen, Tiejun Huang, Timothée Masquelier, and Yonghong Tian. Deep residual learning in spiking neural networks. *Advances in Neural Information Processing Systems (NeurIPS)*, 34, 2021.

[36] Zhaokun Zhou, Yuesheng Zhu, Chao He, Yaowei Wang, Shuicheng YAN, Yonghong Tian, and Li Yuan. Spikformer: When spiking neural network meets transformer. In *International Conference on Learning Representations (ICLR)*, 2023.

[37] Ashish Vaswani, Noam Shazeer, Niki Parmar, Jakob Uszkoreit, Llion Jones, Aidan N Gomez, Łukasz Kaiser, and Illia Polosukhin. Attention is all you need. *Advances in Neural Information Processing Systems (NeurIPS)*, 30, 2017.

[38] Rajat Raina, Anand Madhavan, and Andrew Y Ng. Large-scale deep unsupervised learning using graphics processors. In *International Conference on Machine Learning (ICML)*, pages 873–880, 2009.

[39] Nal Kalchbrenner, Lasse Espeholt, Karen Simonyan, Aaron van den Oord, Alex Graves, and Koray Kavukcuoglu. Neural machine translation in linear time. *arXiv preprint arXiv:1610.10099*, 2016.

[40] Jonas Gehring, Michael Auli, David Grangier, Denis Yarats, and Yann N Dauphin. Convolutional sequence to sequence learning. In *International Conference on Machine Learning (ICML)*, pages 1243–1252. PMLR, 2017.

[41] Eric Martin and Chris Cundy. Parallelizing linear recurrent neural nets over sequence length. In *International Conference on Learning Representations (ICLR)*, 2018.

[42] Mark Harris, Shubhabrata Sengupta, and John D Owens. Parallel prefix sum (scan) with cuda. *GPU gems*, 3(39):851–876, 2007.

[43] Eimantas Ledinauskas, Julius Ruseckas, Alfonsas Juršėnas, and Giedrius Buračas. Training Deep Spiking Neural Networks. *arXiv preprint arXiv:2006.04436*, 2020.

[44] Seongsik Park, Seijoon Kim, Byunggook Na, and Sungroh Yoon. T2fsnn: deep spiking neural networks with time-to-first-spike coding. In *2020 57th ACM/IEEE Design Automation Conference*, pages 1–6. IEEE, 2020.

[45] Saeed Reza Kheradpisheh, Maryam Mirsadeghi, and Timothée Masquelier. Bs4nn: binarized spiking neural networks with temporal coding and learning. *Neural Processing Letters*, 54(2):1255–1273, 2022.

[46] Dongwoo Lew, Kyungchul Lee, and Jongsun Park. A time-to-first-spike coding and conversion aware training for energy-efficient deep spiking neural network processor design. In *Proceedings of the 59th ACM/IEEE Design Automation Conference*, pages 265–270, 2022.

[47] Lina Bonilla, Jacques Gautrais, Simon Thorpe, and Timothée Masquelier. Analyzing time-to-first-spike coding schemes. *Frontiers in Neuroscience*, 16, 2022.

[48] Wei Fang, Yanqi Chen, Jianhao Ding, Ding Chen, Zhaofei Yu, Huihui Zhou, Timothée Masquelier, Yonghong Tian, and other contributors. Spikingjelly. <https://github.com/fangwei123456/spikingjelly>, 2020. Accessed: 2020-10-23.

[49] Friedemann Zenke and Tim P Vogels. The remarkable robustness of surrogate gradient learning for instilling complex function in spiking neural networks. *BioRxiv*, 2020.

[50] Hongmin Li, Hanchao Liu, Xiangyang Ji, Guoqi Li, and Luping Shi. Cifar10-dvs: An event-stream dataset for object classification. *Frontiers in Neuroscience*, 11, 2017.

[51] Ilya Loshchilov and Frank Hutter. Sgdr: Stochastic gradient descent with warm restarts. *arXiv preprint arXiv:1608.03983*, 2016.

[52] Hongyi Zhang, Moustapha Cisse, Yann N Dauphin, and David Lopez-Paz. mixup: Beyond empirical risk minimization. *arXiv preprint arXiv:1710.09412*, 2017.

[53] Sangdoo Yun, Dongyoon Han, Seong Joon Oh, Sanghyuk Chun, Junsuk Choe, and Youngjoon Yoo. Cutmix: Regularization strategy to train strong classifiers with localizable features. In *Proceedings of the IEEE/CVF International Conference on Computer Vision (ICCV)*, pages 6023–6032, 2019.

[54] Samuel G Müller and Frank Hutter. Trivialaugment: Tuning-free yet state-of-the-art data augmentation. In *Proceedings of the IEEE/CVF International Conference on Computer Vision (ICCV)*, pages 774–782, 2021.

[55] Zhun Zhong, Liang Zheng, Guoliang Kang, Shaozi Li, and Yi Yang. Random erasing data augmentation. In *Proceedings of the AAAI conference on artificial intelligence (AAAI)*, volume 34, pages 13001–13008, 2020.

- [56] Christian Szegedy, Vincent Vanhoucke, Sergey Ioffe, Jon Shlens, and Zbigniew Wojna. Rethinking the inception architecture for computer vision. In *Proceedings of the IEEE conference on Computer Vision and Pattern Recognition (CVPR)*, pages 2818–2826, 2016.
- [57] Qingyan Meng, Mingqing Xiao, Shen Yan, Yisen Wang, Zhouchen Lin, and Zhi-Quan Luo. Training high-performance low-latency spiking neural networks by differentiation on spike representation. In *Proceedings of the IEEE/CVF Conference on Computer Vision and Pattern Recognition (CVPR)*, pages 12444–12453, 2022.
- [58] Nitin Rathi and Kaushik Roy. Diet-snn: A low-latency spiking neural network with direct input encoding and leakage and threshold optimization. *IEEE Transactions on Neural Networks and Learning Systems*, 2021.
- [59] Nitin Rathi, Gopalakrishnan Srinivasan, Priyadarshini Panda, and Kaushik Roy. Enabling deep spiking neural networks with hybrid conversion and spike timing dependent backpropagation. In *International Conference on Learning Representations (ICLR)*, 2020.

6 Supplementary Material

6.1 Environments for Simulation Speed Benchmark

The simulation speed benchmark is carried out on a Ubuntu 20.04.6 LTS server with the Intel Xeon(R) Gold 6226R CPU, 192G memory, and the NVIDIA Quadro RTX 6000 (24G) GPU. The PyTorch vision is 1.12.1, the CUDA version is 11.3.1, and the GPU driver version is 525.105.17.

6.2 Parameters Initialization

For the PSN and masked PSN, the weights are initialized by the kaiming uniform. More specifically, the values are initialized from $\mathcal{U}(-\sqrt{5}, \sqrt{5})$. For the SPSN, the weight is initialized by an exponential decay method

$$W_i = 2^{i-k+1}, \quad i = 0, 1, \dots, k-1 \quad (17)$$

which is similar to the weight of the LIF neuron with $\tau_m = 2$ and removing reset. The thresholds of the PSN family are all initialized as 1.

6.3 Implementation of the Sliding PSN

As mentioned in the main text, the sliding PSN can be implemented by both the matrix-matrix multiplication and the 1D convolution. However, the 1D convolution is much slower than the matrix-matrix multiplication, which is caused by:

- 1) The parallelism of convolution is lower than matrix-matrix multiplication, as we can find that the 1×1 convolution is implemented by the fully connected layer in modern deep ANNs.
- 2) The 1D convolution of the SPSN requires the input with a shape of $(\dots, 1, T)$, while the default data format in SpikingJelly is (T, N, \dots) . Thus, the transpose operation has to be used to move the time-step dimension, which copies data and slows down the speed.

6.4 Training Hyper-parameters

The main hyper-parameters for different datasets are shown in Tab.3. Unless otherwise specified, the weight decay (wd) is 0, the momentum is 0.9 for the SGD optimizer, the learning rate scheduler is the cosine annealing schedule [51], the automatic mixed precision training is used, and the surrogate function is the arctan surrogate function $\sigma(x) = \frac{\alpha}{2(1+(\frac{\pi}{2}\alpha x)^2)}$ with $\alpha = 4$ from [13]. Other training options are listed as follows.

Dataset	Optimizer	Batch Size	Epuch	Learning Rate	GPUs	Loss
Sequential CIFAR10/100	SGD AdamW(SPSN)	128	256	0.1 0.001(SPSN)	1	CE
CIFAR10	SGD	128	1024	0.1	1	CE
ImageNet	SGD	64 (SEW-18) 32 (SEW-34)	320	0.1	8	TET
CIFAR10-DVS	SGD, wd=5e-4	32	200	0.1	2	TET

Table 3: Training hyper-parameters for different datasets.

Static/Sequential CIFAR The transforms include random mixup [52] with $p = 1, \alpha = 0.2$, random cutmix [53] with $p = 1, \alpha = 1$, random choice of two mix methods with $p = 0.5$, random horizontal flip with $p = 0.5$, trivial augment [54], normalization, random erasing [55] with $p = 0.1$, and label smoothing [56]. The number of channels is 256 for static CIFAR and 128 for sequential CIFAR.

ImageNet Transforms are identical to [35]. We loaded the pre-trained weights from the standard ResNet provided by the ANN community as better initialized parameters. Similar techniques have been widely used in surrogate training [57, 58, 59].

CIFAR10-DVS Transforms are identical to [28]. We used the almost identical network structure, training hyper-parameters, and options as [28], except that we use the plain BN rather than TEBN.

T	N	\mathcal{M}_{NO}	\mathcal{M}_{IF}	\mathcal{M}_{PSN}	Δ_{IF-NO}	Δ_{PSN-NO}	$\frac{\Delta_{IF-NO}}{\Delta_{PSN-NO}}$	$\frac{\Delta_{IF-NO} - \Delta_{PSN-NO}}{T \cdot N}$
16	16	35129.9	70563.9	53675.9	35434	18546	1.9	66.0
8	16	18935.9	36863.9	28225.9	17928	9290	1.9	67.5
16	8	18933.9	36099.9	28223.9	17166	9290	1.8	61.5

Table 4: Comparison of the memory consumption of training SNNs with the IF neuron and the PSN.

6.5 Memory Consumption of the PSN family

The memory complexity of the SNN during training can be approximated as $\mathcal{O}(\mathcal{W} + T \cdot (\mathcal{X} + \mathcal{H}))$, where \mathcal{W} is the number of synapses such as convolutional/linear layers and weights inside neurons such as \mathbf{W} in the PSN, T is the number of time-steps, \mathcal{X} is the input/output of all layers, and \mathcal{H} is the hidden state of all layers. When comparing the SNN using the vanilla spiking neurons or the PSN family, the difference in memory consumption mainly depends on \mathcal{H} .

For the vanilla spiking neurons, it can be found that the number of hidden states is at least 2, which are \mathbf{H} and \mathbf{V} . The number of hidden states increases if the spiking neuron integrates more complex neuronal dynamics such as adaptative thresholds. While for the PSN, only \mathbf{H} is used and the number of hidden states is 1. Thus, it can be found that the memory consumption of the PSN is $\mathcal{O}(T \cdot N)$ less than the vanilla spiking neurons, where N is the number of neurons in the SNN.

We design an interesting experiment to verify our analysis. We measure \mathcal{M}_{NO} , which is the memory consumption of training the network with only synapses but no neurons to estimate $\mathcal{O}(\mathcal{W} + T \cdot (\mathcal{X}))$. Then we measure \mathcal{M}_{IF} and \mathcal{M}_{PSN} , which are SNNs with the simplest vanilla spiking neuron, the IF neuron, and the PSN to estimate $\mathcal{O}(\mathcal{W} + T \cdot (\mathcal{X} + \mathcal{H}))$. Thus, we can estimate the memory consumption of hidden states in two SNNs by $\Delta_{IF-NO} = \mathcal{M}_{IF} - \mathcal{M}_{NO}$ and $\Delta_{PSN-NO} = \mathcal{M}_{PSN} - \mathcal{M}_{NO}$. We test on the VGG-11 structure, and the results are shown in Tab.4. It can be found that the $\Delta_{PSN-NO} < \Delta_{IF-NO}$, and $\frac{\Delta_{IF-NO}}{\Delta_{PSN-NO}} \approx 2$ in all cases, which matches our analysis. More specifically, the IF neuron uses 2 hidden states, and the PSN uses 1 hidden state, then the ratio of their extra memory consumption should be 2. It can also be found that $\frac{\Delta_{IF-NO} - \Delta_{PSN-NO}}{T \cdot N}$ is approximately a constant, which also corresponds to our analysis that the memory consumption of the PSN is $\mathcal{O}(T \cdot N)$ less than the IF neuron.